Impact crater degradation, Oxia Planum, Mars

Journal of Maps

ISSN: (Print) (Online) Journal homepage: https://www.tandfonline.com/loi/tjom20

Impact crater degradation, Oxia Planum, Mars

Amelie L. Roberts, Peter Fawdon & Melissa Mirino

To cite this article: Amelie L. Roberts, Peter Fawdon & Melissa Mirino (2021) Impact crater degradation, Oxia Planum, Mars, Journal of Maps, 17:2, 569-578, DOI: 10.1080/17445647.2021.1976685

To link to this article: https://doi.org/10.1080/17445647.2021.1976685

JOURNAL OF MAPS
2021, VOL. 17, NO. 2, 569–578
https://doi.org/10.1080/17445647.2021.1976685

SCIENCE

OPEN ACCESS Check for updates

Impact crater degradation, Oxia Planum, Mars

Amelie L. Roberts [a], Peter Fawdon [b] and Melissa Mirino [b]

[a]School of Earth and Environmental Sciences, St. Andrews University, St. Andrews, UK; [b]School of Physical Sciences, Open University, Milton Keynes, UK

ABSTRACT

The main goal of the European Space Agency (ESA) and Roscosmos ExoMars rover mission is to collect samples from the near-subsurface of Mars. The rover will look for any physical or chemical evidence of ancient life in the near subsurface. This map shows the distribution of impact craters at this proposed landing site in Oxia Planum on Mars. The map records 1199 impact craters > 500 m in diameter in a 5.0° × 2.5° region around Oxia Planum. The impact craters are symbolised based on the way different aspects of their morphology have degraded since their formation. The distribution of degradation and burial morphologies of impact craters can be used to determine where burial and erosion processes have occurred. Because the formation of impact craters is well constrained, occurs instantly and with a predictable flux, future studies could use this knowledge and our dataset to constrain when these events occurred.

ARTICLE HISTORY
Received 26 January 2021
Revised 27 August 2021
Accepted 28 August 2021

KEYWORDS
Oxia Planum; ExoMars; craters; impact craters; crater database; impact crater degredation

1. Introduction

We have mapped the distribution of impact degradation states for 1199 impact craters >500 m in diameter in a 5.0° × 2.5° region at Oxia Planum, Mars, the proposed landing site of the European Space Agency (ESA) ExoMars rover. The aim of the ExoMars rover, 'Rosalind Franklin', is to collect samples from the near-subsurface looking for any physical or chemical evidence of ancient life on Mars (Vago et al., 2017). The landing site, and our study area, are located on the transition between the ancient (> 3.7 Ga; Noachian age) Arabia Terra region and the low lying younger surface (< 3.0 Ga; Amazonian) of Chryse Planitia to the northwest (Figure 1). This area is important for ESA and Roscosmos's rover mission due to the identification of a widespread clay-bearing unit which is the primary target of astrobilogical interest for the rover (Carter et al., 2016; Mandon et al., 2021; Quantin-Nataf et al., 2021). The current interpretations attribute this unit to either subaqueous to subaerial emplacement of clays (Mandon et al., 2021) or aqueous alterations of the Noachian terrain (Quantin-Nataf et al., 2021). With the current understanding of resources to support life, liquid water in a lithosphere-hydrosphere system is likely the most basic requirement to cause a planet to be habitable (Southam et al., 2015; Vago et al., 2017). The clay-bearing unit likely represents such an environment from which the rover will collect samples.

The stratigraphy, burial and degradation state of impact craters in this area are important for the ExoMars mission. Firstly, impact crater populations are commonly studied to assess planetary surface ages and resurfacing processes (Hartmann & Neukum, 2001; Ivanov et al., 2002; Neukum et al., 2001). Thus, the distribution and burial of impact craters can tell us where and when burial has occurred (Quantin-Nataf et al., 2019). Secondly, small, young craters expose deeper layers in the crater walls that can be accessed by the Martian rover (Vago et al., 2017). Furthermore, the distribution of rayed craters, craters retaining fine grained ejecta as radial streaks from the impact zone, may be important for identifying the source of float rocks and possible traversability hazards observed by the rover (Newsom et al., 2015). Finally, for craters 5–10 km in diameter (the largest craters in our study), interactions of groundwater with thermal energy caused by the impact could have created long-lasting environments that may have once supported life (Osinski et al., 2013; Schwenzer et al., 2012).

Many classification systems have been created for categorising impact craters on Mars (e.g.: Barlow, 2005; Barlow et al., 2000; Barlow & Bradley, 1990; Grant & Schultz, 1993; Strom et al., 2018). These classifications systems, such as Robbins and Hynek (2012) investigate larger craters in global data sets with a data resolution of 100 m/pixel. Similarly for previous landing sites, crater degradation has been classified based on regional and global classifications and degradation rates focusing on the morphologies

CONTACT Peter Fawdon peter.fawdon@open.ac.uk School of Physical Sciences, Open University, Milton Keynes, Buckinghamshire MK7 6AA, UK
@DrPFawdon

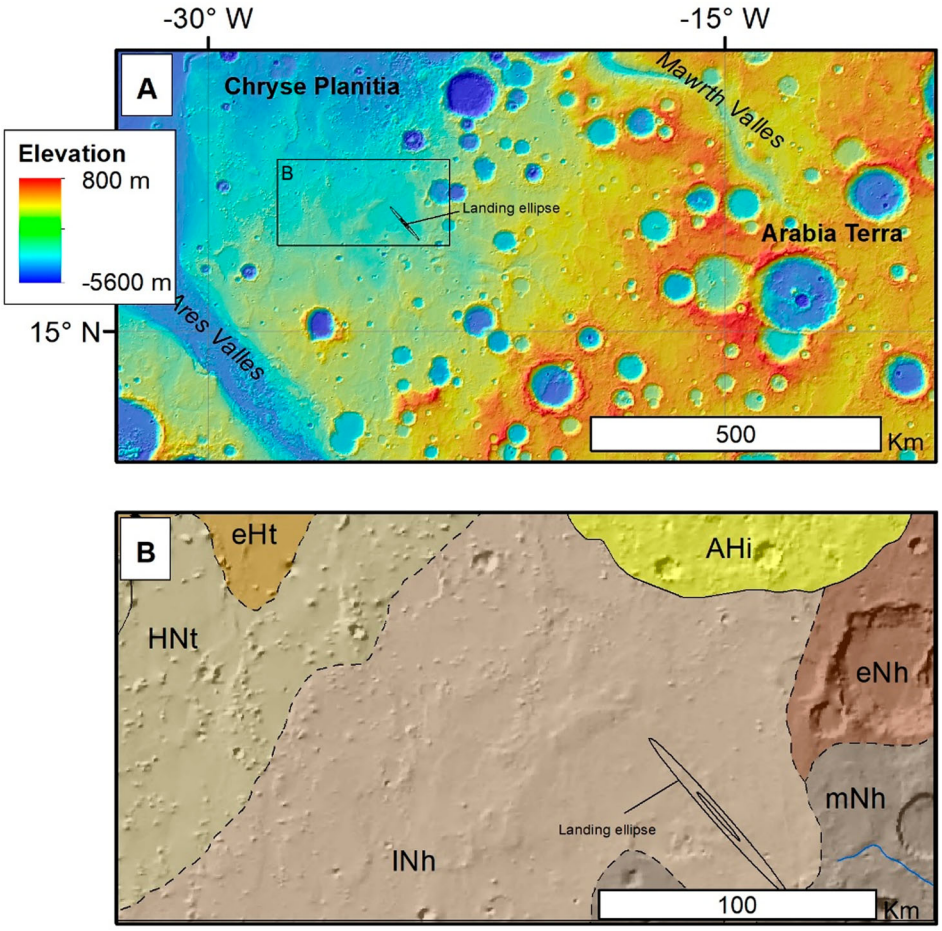

Figure 1. Location and context.

Mapping area extent in (a) regional geological context, (b) local context and the geological map of Mars (Tanaka et al., 2014a). The study area is shown with the topography at ~463 m/pixel in Mars Orbiter Laser Altimeter (MOLA) Digital Elevation Model (DEM); blue is low and red is high and the location of the ExoMars 2020 rover landing ellipse outlined in black.

of ejecta blankets and crater rims in particular (Golombek et al., 2016; Sweeney et al., 2016). Here we have developed a classification scheme for higher resolution data (5–6 m/pixel) available in Oxia Planum, differing from previous surveys (eg: Barlow, 2005; Barlow et al., 2000; Barlow & Bradley, 1990; Robbins & Hynek, 2012; Strom et al., 2018) who use lower resolution data sets and consider the whole of Mars. At the scale of CTX imagery, degradation morphologies (and the processes by which they occur) have more of an impact on the observed crater morphology than differences in shape caused by the initial formation of the crater. Consequently, it is important to record this and the distribution of these different erosion morphologies in more detail to understand the geological history of the area and the process which have affected the clay bearing unit which is important for this study and the ESA and Roscosmos's ExoMars 2022 rover mission. Here, we focus on each individual morphology of a crater such as the rim, ejecta, cross-sectional shape and stratigraphic relationship and assess their relative degradation state to what would be expected for a fresh impact crater in Oxia Planum.

2. Materials and methods

2.1. Location and projection

The main map is located between 17.5–20.0°N and 23.0–28.0°W (337–332°E) (Figure 1) at Oxia Planum and was created in an Equidistant Cylindrical Projection supplied by the USGS. The area is 300 km by 150 km with an area of 45,000 km^2 and elevation ranging between −2365 and −3795 m relative to the MOLA datum. This area is predominantly located in Arabia Terra. The Late Noachian highland unit (lNh) dominates this area with small portions of the Hesperian and Noachian transition (HNt) and Early Hesperian transitional (eHt) units to the west on the margin of Chryse Planitia and part of the Middle and Early Noachian highland (mNh, eNh) units to the east (Tanaka et al., 2014b). The ~100 × ~10 km landing ellipse for the ExoMars rover mission (Vago et al., 2017) is also within the study area.

2.2. Data

2.2.1. Data in the visible spectrum

The qualitative analysis was performed in ArcGIS10.1 primarily using data from the Context Camera (CTX;

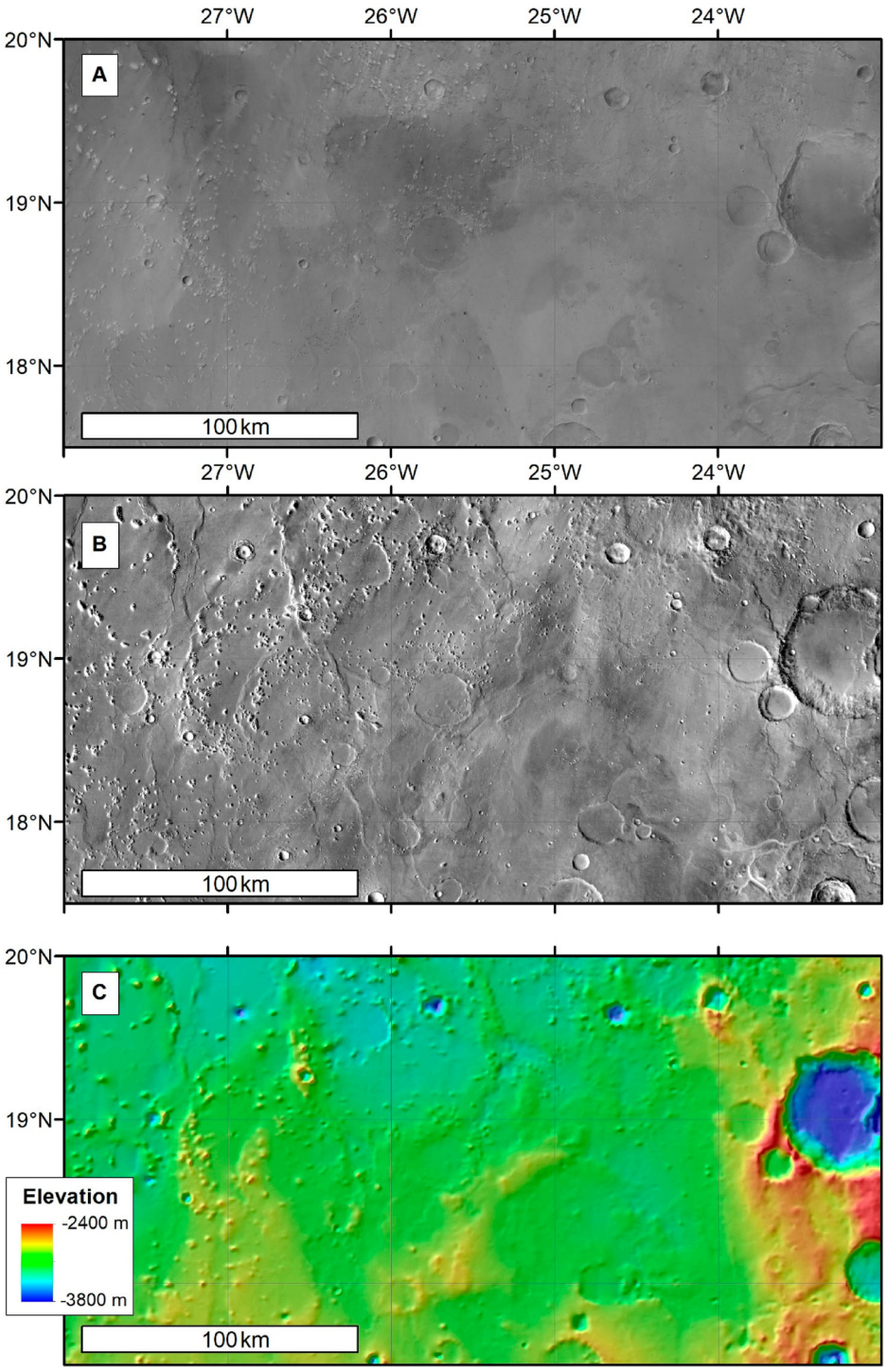

Figure 2. Basemaps.

Basemap data used in this study; (A) ~6 m/pixel CTX mosaic from (Dickson et al., 2018). (B) ~100 m/pixel THEMIS daytime mosaic. (C) ~463 m/pixel MOLA DEM overlying a hillshade model.

Malin et al., 2007) instrument on the Mars Reconnaissance Orbiter (MRO) imaging at wavelengths between 500 and 700 nm with a pixel size of ~6 m. Individual CTX images were used for identifying crater morphologies with digitisation being performed against the seam-corrected and seam-mapped Murray Lab global CTX mosaic tiles E028N16 and E024N16, of beta01 (http://murray-lab.caltech.edu/CTX/index.html; Dickson et al., 2018).

2.2.2. Thermal data products

The Thermal Emission Imaging System camera (THEMIS; Christensen et al., 2004; Edwards et al., 2011) records visible wavelengths between 420 and 860 nm and thermal data at wavelengths between 6800 and 14,900 nm as part of the 2001 Mars Odyssey Orbiter. The data from ~100 m/pixel daytime quadrangle mosaic Oxia Palus, 00N315E, was used as a lower resolution dataset overlain by the MOLA data for the

Table 1. Stratigraphic relationship. *The stratigraphic relationship between the impact crater and the underlieing terrain in Oxia Planum. This relationship describes the age of the crater relative to the surrounding Martian surface.*

Type	Example	Description	Interpretation
Underlying	*18°45′30″N, 27°36′0″W*	The entire cross-section of the crater has been covered by the same rock units as the surrounding terrain. The rim and ejecta are indistinguishable. The initial shape of this crater can range from bowl, flat and ghost depending on whether the likeness of the crater is retained by the covering stratigraphic unit. Craters are inferred from either features that follow circular paths or a circular topographic low.	An impact that occurred before the formation of the adjacent terrain. This crater has been completely buried and potentially eroded by resurfacing processes.
Embedded	*18°0′0″N, 24° 44′0″W*	These craters are partially covered by either a similar or different rock-type to the surrounding terrain. One key distinguishing feature from the underlying craters is that part of the original crater morphology is preserved I.E parts of the rim.	The impact is at the same stratigraphic level as the surrounding terrain. The crater has been infilled but not buried by subsequent processes.
Overlying with Surficial Deposits	*18°38′30″N, 24°12′30″W*	These craters are superposed on the surrounding terrain. These craters differ from the overlying craters (see overlying) as they contain some deposits inside the crater bowl. Most of the morphology of these crater remain intact.	These craters occurred after the formation of the adjacent terrain. The deposits found inside these craters could be from a range of different sedimentary processes such as windblown sediments from aeolian erosion or ejecta from nearby subsequent craters.
Overlying	*17°31′30″N, 26°6′0″W*	These craters are superposed on the surrounding terrain with minimal to no surficial deposits	These craters occurred after the formation of the adjacent terrain and are relatively young to not have been significantly filled with surficial deposits from aeolian erosion or ejecta from surrounding craters.

identification of topographic subtleties associated with larger craters.

2.2.3. Topographic data

The gridded 463 m/pixel MOLA Digital Elevation Model (DEM; Figure 2) (MOLA; Smith et al., 2001) was used to identify the crater floor topographic profile for larger craters. This data was also used, in conjunction with THEMIS data, for the identification of topographic subtleties associated with the burial of crater rims ('ghost craters', e.g.; Cruikshank et al., 1973). Due to the interpolation between laser altimeter ground tracks, parts of this data are not suitable for observations of craters smaller than 10 km so these smaller craters were found using visual data. This data was also used as a base map.

2.3. Digitisation and errors

Impact crater rims were digitised as vector polygons in ESRI ArcMap 10.1 Geographic Information System Software to the CTX mosaic data. Impact crater rims were drawn with vertex spacing of 25 m at a scale of 1:15,000. In cases where the crater rim was removed, or artefacts in the CTX mosaic obscured the rim, a best estimate was made based on a circular perimeter. As this is qualitative analysis, consequently there may be random errors associated with the digitisation. In particular, craters which are embedded or overlying with surficial deposits can be quite similar (e.g.; Table 1, rows 2 and 3). Identification and digitisation errors can occur from the CTX image mosaics. Errors arise from inconsistent georeferencing and colour balance compared with the original CTX images. In particular, when an impact crater was positioned on an image seam, parts of or the entire crater could be lost due to stitching. To mitigate against this we used the original mosaiced CTX images for classification and THEMIS to correct for errors in position. In addition, as only visual identification was used to identify ghost craters <10 km, there may be a larger number of ghost craters which could not be identified without the topographic data available at that scale.

2.4. Making the map

The Map of Impact Crater Degradation at Oxia Planum, Mars was created to be presented at a scale of 1:275,000 to allow for the visualisation of the smallest craters (~ 500 m) included in the survey (sample version shown in Figure 3). The MOLA data (Section 2.2.3) was used as the base map which was overlain by a MOLA hillshade and slope map at 60% transparency. Another MOLA DEM hillshade was overlain on top of the vector files of the map at 90% transparency along to show details across the crater polygon shape file. The ejecta were represented by creating a buffer of one tenth of the perimeter of the craters and shaded by crosshatch. Crater rims, cross-sectional shape and stratigraphy were represented by lines, shading, and colour.

2.5. Impact crater classifications

A classification scheme was developed based on the post-impact burial and degradation of four aspects of impact crater morphology (Figure 3). The following tables: (Table 1) stratigraphic relationship, (Table 2) cross-sectional shape, (Table 3) rim morphology, and (Table 4) ejecta morphology show examples,

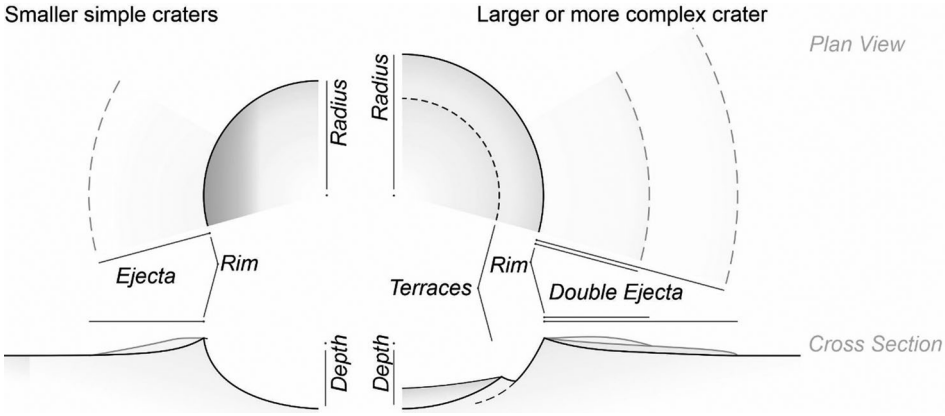

Figure 3. Idealised fresh crater structure.
Illustration of the generalised structure of an idealised fresh impact crater.

Table 2. Crater floor cross section. *The cross sectional shape of the impact crater floor shows if the crater has been infilled or buried and if the floor has been exhumed through differential erosional processes.*

Type	Example	Description	Interpretation
Ghost	*19°02′00″N, 25° 01′00″W*	Craters with cross-section shapes that have elevation changes indistinguishable from the surrounding terrain. None of the original crater morphology can be directly observed. Craters are inferred by overlying low relief ridges that follow or are deflected into a circular pattern.	Impact craters that occurred before significant burial events.
Inverted	*18°19′00″N, 24° 22′30″W*	Circular plateaus that are partially or completely elevated compared with the surrounding topography.	Impact craters that have formed, been infilled by a more resistant material than the bedrock, and have subsequently undergone differential erosion to create the inverted crater morphology.
Flat	*18°28′00″N, 24.53′30″W*	Craters with a flat floor cross section. These differ from Ghost craters as the terrain is flat and has a distinguishable difference in elevation or shape to the surrounding terrain.	These impact craters have been infilled and subsequently eroded. This erosion has likely been controlled by the rim causing a slight difference in elevation between the crater and the surrounding terrain.
Bowl	*19°39′0″N, 26° 55′0″W*	Craters where the excavated cavety has not been infilled, which for a simple crater most relvent to this study is a bowl-like cross section. Larger examples may include a central peak or pit, and terraced walls.	Impact craters that have not been infilled, eroded or buried. These are young craters that retain a near-original morphology.

descriptions, and interpretations of the impact craters found in the study area.

3. Results

The distribution and degradation of 1999 craters in Oxia Planum are shown in a sample map (Figure 4) and the Map of Impact Crater Degradation at Oxia Planum, Mars. No rayed craters were found in this study area larger than 500 m wide in diameter. However, rayed craters smaller than 500 m in diameter exist in Oxia Planum (e.g.: 18°20′30″N, 24°6′0″W) and there are possibilities for these craters to be included in further studies of the area at a smaller scale.

4. Discussion

4.1. Occurance of degradation types in Oxia Planum

The classification scheme of degradation type allows for 64 different permutations. However, many of these permutations are unlikely to occur together. For example, if a crater underlies the stratigraphy then the crater cannot have a visible sharp or embayed rim or any visible ejecta as each of these morphologies have been subsequently covered. In Oxia Planum, we find that only 40 meaningful permutations occur (Table 5). Some permutations, such as rayed ejecta with a sharp rim and bowl shape can occur but are not visible in Oxia Planum at this scale. Rays were included as a category in this research because they represent an end member morphology and indicate the potential range of discontinuous ejecta. Future studies of the area could be expanded for smaller craters which would then include a number of craters in this category (e.g.: 18°20′30″N, 24°6′0″W).

In Oxia Planum, ‘Overlying’ craters (Table 1; ‘Overlying’) represent the youngest craters and account for 20.17% of craters. The most common crater morphologies associated with this category are a sharp rim, bowl shape and removed ejecta which account for 8.42% of all craters. Craters with sharp rims, continuous ejecta, and a bowl shape represent the least degraded craters accounting for 2.50% of all craters. The largest least

Table 3. Crater rim morphology. *The morphology of the impact crater rim reflects a range of degradation and burial processes that have acted on a specific part of the crater.*

Type	Example	Description	Interpretation
Removed	*18°54′30″N, 25°18′30″W*	Craters where the original rim is unidentifiable.	Impact craters where the upstanding part of the crater rim has been eroded and/or buried.
Muted	*17°45′00″N, 26°47′30″W*	There is topographic evidence of where the rim is or was but the rim no longer retains its sharp peaks.	The crater rim and floor has been covered by deposits thick enough to bury the relief the crater had at the time but insufficient to mask where the initial crater rim was. Subsequent erosion could also have removed the sharp peaks of the crater rim.
Embayed	*19°29′00″N, 24°11′30″W*	The crater rim is partially overlain (or removed and overlain).	Part of the crater rim has been buried or removed due a depositional process. This may be related to water and sedimentation, volcanism or fluidised ejecta.
Sharp	*19°37′00″N, 24°14′00″W*	The original uplifted crater rim is upstanding and clearly defined.	The crater rim has not experienced any significant degradation that would alter it from its original state.

Table 4. Ejecta morphology. *The morphology of impact ejecta can be used to compare the effects of low intensity erosion on craters of comparable size (Arvidson et al., 1976). This is because ejecta is generally poorly consolidated and relatively easy to erode but the amount of it changes with impact crater diameter.*

Type	Example	Description	Interpretation
Removed	*19°54′0″N, 25°37′30″W*	The crater ejecta cannot be observed.	The ejecta has either been completely eroded and/or buried.
Discontinuous	*18°0′30″N, 24°15′30″W*	There is material in the area where the impact ejecta is expected to be but it forms an incomplete layer. Remnant ejecta is seen preferentially degraded both proximally and distally with respect to the crater rim.	Continuous impact ejecta that has been partially removed by erosion processes. This suggest that these craters are older than craters of the same size with more complete ejecta blankets.
Continuous	*17°27′30″N, 23°1′30″W*	The crater ejecta is visible and shows few to no signs of degradation. Some ejecta may have a small number of impact craters but otherwise the ejecta blanket remains continuous.	The ejecta has not been eroded or removed. Thus, the crater is young relative to other craters of the same size that are experiencing a similar erosional regime.
Rayed	*18°20′30″N, 24°6′0″W*	Impact craters with radial lines of either light or dark material	The preservation of the rays are observed where fine material has been removed by the shock of the impact and not yet removed or covered by dust.

degraded crater in the area is the 16 km 'Kilkhampton Crater' (17.52 °N, 32.3° E). This is the only crater of its diameter to exhibit a variety of less degraded morphologies.

'Overlying with surficial deposits' craters (Table 1; 'Overlying with Surficial Deposits') represent the second youngest craters in Oxia Planum and show some erosion from aeolian and surficial processes which have led to partial infilling of sediment. These craters are the most common and account for 42.08% of all craters in Oxia Planum. Of these, the most common features were a bowl shape, a muted rim, and removed ejecta which account for 25% of all craters and were the most commonly observed crater in Oxia Planum.

'Embedded' craters (Table 1; 'Embedded') account for 10.92% of craters in Oxia Planum and are at the same stratigraphic level as the light-toned layer predominantly found in the Late Noachain Highland unit (Figure 1(c)). These have subsequently been filled by a local depostional process, Quantin-Nataf et al. (2021) suggests that sedimentation or some other active flow such as explosive deposits or lava flows are all plausible processes that may have occured to infill crater floors.

'Underlying' craters (Table 1; 'Underlying') are the oldest of the commonly observed morphologies and account for 26.83% of craters in Oxia Planum. These craters have non-visible or muted rims, non-visible ejecta and have been completely buried by a layer sufficiently thick to overcome any remnant rim and to completely infill the original crater floor. It appears these craters were formed before layered terrains and parts of the clay-bearing unit and are thus the oldest craters observed in the mapping area.

Craters with discontinuous ejecta blankets with bowl shaped cross-section and 'Overlying' with both surficial and no surficial deposits are also commonly observed at 11.67% of all craters in Oxia Planum. These craters are important because of any discontinuous ejecta associated with them. Whilst this is not observable in the CTX data, such ejecta may provide a source of interesting outcrops for the ExoMars rover to observe or a set of navigational hazards if it lands near to one of these craters.

4.2. Comparison with other crater surveys

Many previous classification systems have categorised the degradation of craters by qualitative observations using the morphologies such as the rim and ejecta (e.g.; Robbins & Hynek, 2012) while others quantitatively looked at crater depth-to-diameter ratio, numerically representing each crater's cross-sectional shape (e.g; Barlow, 2005; Robbins & Hynek, 2012). The findings of our approach, which show the likelihood of common morphologies of

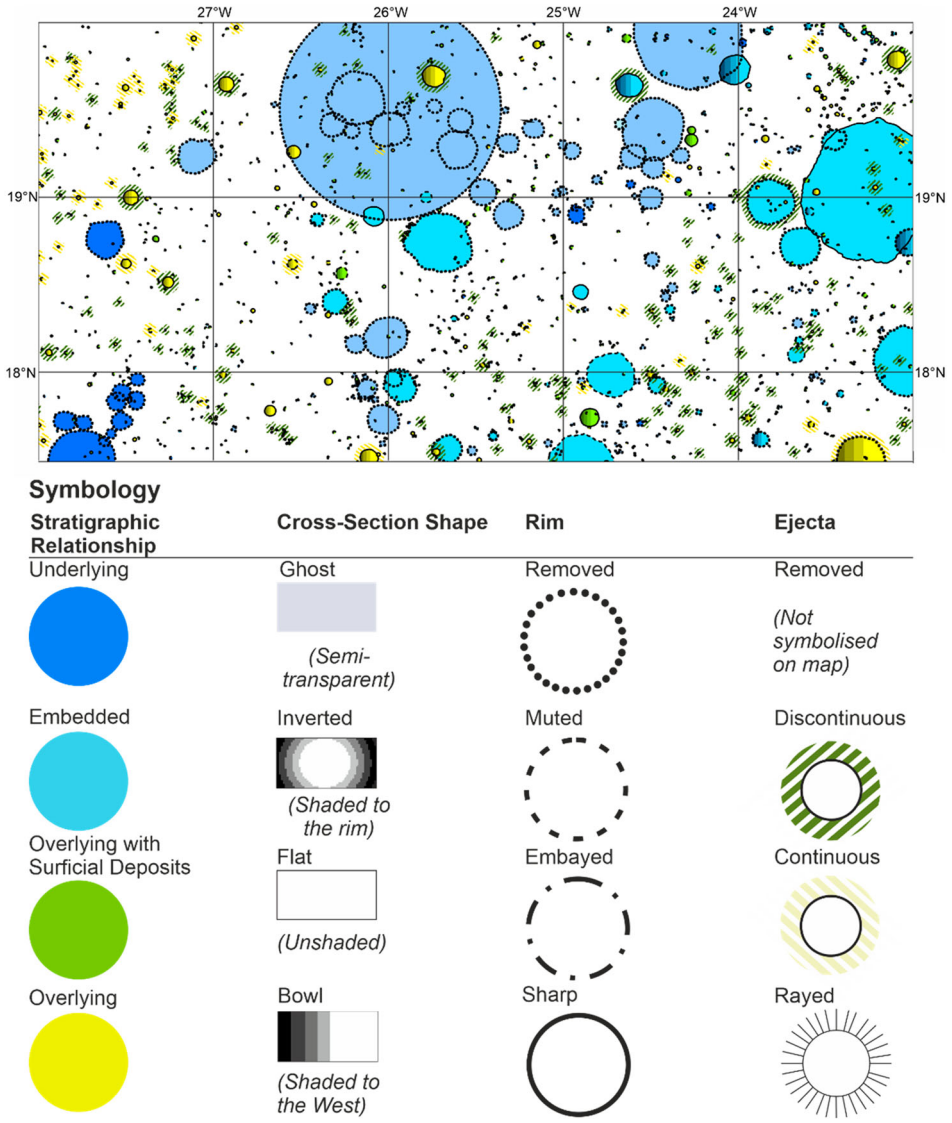

Figure 4. Sample map and symbology.

A sample version of the Main Map showing the distribution of impact craters in the study area and an abridged legend with the symbols used to illustrate the variations in degradation morphology.

different crater characteristics being observed together (Table 5), are reflected in the classifications. Impact craters with these degradation trends are commonly observed throughout the southern hemisphere of Martian terrain, thus crater degradation observed at Oxia Planum is consistent with other Martian terrains.

The crater morphologies in Oxia Planum with the bowl shape, sharp rims, and continuous or rayed ejecta are morphologies represented in the most 'pristine' class (class 4; Robbins & Hynek, 2012). Unlike the pristine craters, more degraded craters observed in Oxia Planum are represented in some classification schemes (Barlow, 2005; Robbins & Hynek, 2012). These classification systems do not identify which of the crater characteristics is degraded and will group the entire crater into one class even if only one morphology is eroded such as an eroded ejecta blanket while the rest of the characteristics may remain pristine (class 3; Robbins & Hynek, 2012). Another feature these classification systems do not capture is whether the crater has been embedded, embayed or inverted and, if infilling or embayment has been observed. Such craters are classified with the eroded craters as 'heavily degraded' (class 2; Robbins & Hynek, 2012). Other classification schemes also rely on the processes that have affected the craters whereas our classification does not. The classification scheme by Grant and Schultz (1993) does account for the embayed and embedded craters observed in Oxia Planum which were found to be common throughout the Martian surface. However, this classification scheme does not represent the different degradation states of craters and does not consider the different range of morphologies for different crater characteristics such as the inverted craters which are common in the Oxia Planum region at this scale of observation. Our classification accounts for the different degradation morphologies of different crater characteristics and additional features such as infilling in the stratigraphic

Table 5. Percent of each crater type. *The percent of each occurrence of each crater type in the mapping area extent given in order of most abundant for each stratigraphic relationship. Percents were calculated from the number of each crater occurrence over the total number of craters. Craters which occurred at frequencies higher than 1% were increasingly shaded from 1% to the highest percentage, 25.25%.*

Statigraphic Relationship	Cross-section	Rim	Ejecta	Crater (n)	Percent (%)
TOTAL UNDERLYING				**322**	**26.83**
Underlying	Ghost	Removed	Removed	233	19.42
Underlying	Bowl	Muted	Removed	42	3.50
Underlying	Flat	Removed	Removed	17	1.42
Underlying	Ghost	Muted	Removed	14	1.17
Underlying	Inverted	Removed	Removed	7	0.58
Underlying	Bowl	Removed	Removed	6	0.50
Underlying	Bowl	Muted	Removed	1	0.08
Underlying	Flat	Muted	Removed	1	0.08
Underlying	Inverted	Muted	Removed	1	0.08
TOTAL EMBEDDED				**131**	**10.92**
Embedded	Bowl	Muted	Removed	42	3.50
Embedded	Flat	Removed	Removed	21	1.75
Embedded	Bowl	Sharp	Removed	15	1.25
Embedded	Bowl	Removed	Removed	12	1.00
Embedded	Bowl	Embayed	Removed	11	0.92
Embedded	Ghost	Removed	Removed	9	0.75
Embedded	Inverted	Removed	Removed	8	0.67
Embedded	Flat	Muted	Removed	5	0.42
Embedded	Flat	Sharp	Removed	3	0.25
Embedded	Ghost	Muted	Removed	3	0.25
Embedded	Bowl	Sharp	Discontinuous	1	0.083
Embedded	Flat	Removed	Discontinuous	1	0.083
TOTAL OVERLYING WITH SURFICIAL DEPOSITS				**505**	**42.08**
Overlying with Surficial Deposits	Bowl	Muted	Removed	303	25.25
Overlying with Surficial Deposits	Bowl	Sharp	Removed	73	6.08
Overlying with Surficial Deposits	Bowl	Removed	Removed	46	3.83
Overlying with Surficial Deposits	Bowl	Muted	Discontinuous	45	3.75
Overlying with Surficial Deposits	Bowl	Sharp	Discontinuous	15	1.25
Overlying with Surficial Deposits	Bowl	Removed	Discontinuous	13	1.08
Overlying with Surficial Deposits	Bowl	Muted	Continuous	3	0.25
Overlying with Surficial Deposits	Flat	Muted	Removed	3	0.25
Overlying with Surficial Deposits	Bowl	Removed	Continuous	2	0.17
Overlying with Surficial Deposits	Flat	Muted	Discontinuous	1	0.08
TOTAL OVERLYING				**242**	**20.17**
Overlying	Bowl	Sharp	Removed	101	8.42
Overlying	Bowl	Sharp	Discontinuous	49	4.08
Overlying	Bowl	Sharp	Continuous	30	2.50
Overlying	Bowl	Muted	Removed	28	2.33
Overlying	Bowl	Muted	Discontinuous	14	1.17
Overlying	Bowl	Muted	Continuous	13	1.08
Overlying	Bowl	Removed	Discontinuous	4	0.33
Overlying	Bowl	Removed	Removed	2	0.17
Overlying	Bowl	Removed	Continuous	1	0.08

relationship, embayment in the crater rim, or inversion in the crater shape characteristics.

5. Conclusions

In this study, we used CTX (5–6 m/pixel) data to map and classify 1199 impact craters > 500 m in diameter at Oxia Planum, Mars, the landing site for the ExoMars 2022 mission. We developed a classification system that categorised craters based on observations of how four aspects of their morphology deviated from the pristine 'fresh' crater morphology. We observed the modification of the ejecta, rim, cross-sectional shape, and relationship with local geological units.

The most commonly occurring craters in Oxia Planum were the craters which were 'Overlying with Surficial Deposits' of which a bowl shape, muted rim and removed ejecta were the most common. Craters underlying the stratigraphy were the second most common at 26.83%, where the ghost cross-sectional shape was the most common amongst these. This was followed by craters 'Overlying' the stratigraphy at 20.17%, followed by craters embedded within the stratigraphy at 10.92%.

This map indicates that certain types of degradation morphology are likely to be found together suggesting that degradation occured heterogeneously through the geological history of Oxia Planum. Future publications using this categorisation system and catalogue will explore these trends to help understand the geological history at the ExoMars landing site.

We present this data as a map and GIS-ready dataset to aid the understanding of impact crater degradation and geological process at the transition between Arabia Terra and Chryse Planitia.

Open Scholarship

Data availability statement

All the data used in this map is freely available. Crater linework data is available as a shape file (.shp) and associated layer (.lyr) file containing the symbology information from The Open University research repository ORDO (https://ordo.open.ac.uk) using the search term 'Oxia Planum Impact Craters' or DOI: 10.21954/ou.rd.13625753. The Context Camera data used for crater observations are available using the Mars Image Explorer (http://viewer.mars.asu.edu/planetview/inst/ctx/#T=0). Base map layers for the map sheet are available from the USGS Astrogeology Science Center for THEMIS (https://astrogeology.usgs.gov/search/map/Mars/Odyssey/THEMIS-Day-IR-Controlled-Mosaic/Mars-THEMIS-Day-IR-Controlled-Mosaic-Oxia-Palus-00N-315E-100mpp) and MOLA gridded hill shade (https://astrogeology.usgs.gov/search/map/Mars/Topography/HRSC_MOLA_Blend/Mars_HRSC_MOLA_BlendShade_Global_200mp_v2).

Software

ArcGIS® 10.5 was used to digitise the data and CorelDrawX7 was used to make the final map product. The degradation likelihood association where calculated using the open-source Anaconda Software using the Python/R data science packages (https://www.anaconda.com/distribution/).

Acknowledgements

We thank S. Mikhail and C. Cousins at St Andrews for initial encouragement; Matt Balme and Jack Wright at the Open University for bureaucratic support and editorial input. We would like to thank reviewers L. Mandon, D. Crown, and B. Marston for their suggested edits which have significantly improved the manuscript and maps. Finally, we thank all the scientists and engineers who built CTX and have operated it for over a decade at Malin Space Science Systems and the Jet Propulsion Laboratory, and D Quinn at the Murray Lab for compiling the CTX mosaic dataset.

Disclosure statement

No potential conflict of interest was reported by the author(s).

Funding

This work was supported by the Open University Space Strategic Research Area for funding A. Roberts throughout her internship and M. Mirino during her PhD. P. Fawdon was funded though UKSA [grant number ST/R001413/1, ST/W002736/1].

ORCID

Amelie L. Roberts http://orcid.org/0000-0001-6504-3085
Peter Fawdon http://orcid.org/0000-0003-1900-8347
Melissa Mirino http://orcid.org/0000-0003-2425-0269

References

Arvidson, R. E., Coradini, M., Carusi, A., Coradini, A., Fulchignoni, M., & Federico, C. (1976). Latitudinal variation of wind erosion of crater ejecta deposits on Mars. *Icarus*, *27*(4), 503–516.

Barlow, N. G. (2005). A review of Martian impact crater ejecta structures and their implications for target properties. *Special Paper of the Geological Society of America*, *384*. https://doi.org/10.1130/0-8137-2384-1.433

Barlow, N. G., Boyce, J. M., Costard, F. M., Craddock, R. A., Garvin, J. B., Sakimoto, S. E. H., Kuzmin, R. O., Roddy, D. J. & Soderblom, L. A. (2000). Standardizing the nomenclature of Martian impact crater ejecta morphologies. *Journal of Geophysical Research E: Planets*, *105*(E11), https://doi.org/10.1029/2000JE001258

Barlow, N. G., & Bradley, T. L. (1990). Martian impact craters: Correlations of ejecta and interior morphologies with diameter, latitude, and terrain. *Icarus*, *87*(1), 156–179. https://doi.org/10.1016/0019-1035(90)90026-6

Carter, J., Quantin, C., Thollot, P., Loizeau, D., Ody, A., & Lozach, L. (2016, March 21-25). *Oxia Planum, a Clay-Laden landing site proposed for the Exomars rover mission: Aqueous mineralogy and alteration scenarios*. 47th Lunar and Planetary Science Conference, held in the Woodlands, Texas.

Christensen, P. R., Jakosky, B. M., Kieffer, H. H., Malin, M. C., McSween, H. Y., Nealson, K., Mehall, G. L., Silverman, S. H., Ferry, S., Caplinger, M. & Ravine, M. (2004). The thermal emission imaging system (THEMIS) for the mars 2001 Odyssey mission. *Space Science Reviews*, https://doi.org/10.1023/b:spac.0000021008.16305.94

Cruikshank, D. P., Hartmann, W. K., & Wood, C. A. (1973). Moon: "Ghost" craters formed during mare filling. *The Moon*, *7*(3–4), https://doi.org/10.1007/BF00564645

Dickson, J. L., Kerber, L. A., Fassett, C. I., & Ehlmann, B. L. (2018, March 19-23). *A global, blended CTX mosaic of mars with vectorized seam mapping: A new Mosaicking pipeline using principles of non-destructive image editing*. 49th Lunar and Planetary Science Conference, held in the Woodlands, Texas.

Edwards, C. S., Nowicki, K. J., Christensen, P. R., Hill, J., Gorelick, N., & Murray, K. (2011). Mosaicking of global planetary image datasets: 1. Techniques and data processing for thermal emission imaging system (THEMIS) multi-spectral data. *Journal of Geophysical Research E: Planets*, *116*(10), https://doi.org/10.1029/2010JE003755

Golombek, M. P., Warner, N., Daubar, I. J., Kipp, D., Fergason, R., Kirk, R., Huertas, A., Beyer, R., Piquex, S., Putzig, N. E., Calef, F. & Banerdt, W. B. (2016, March 21-25). *Surface and subsurface characteristics of western Elysium Planitia, Mars*. 47th Lunar and Planetary Science Conference, held in the Woodlands, Texas.

Grant, J. A., & Schultz, P. H. (1993). Degradation of selected terrestrial and Martian impact craters. *Journal of Geophysical Research*, *98*(E6), 11025. https://doi.org/10.1029/93je00121

Hartmann, W. K., & Neukum, G. (2001). Cratering chronology and the evolution of Mars. *Space Science Reviews*, *96*. https://doi.org/10.1023/A:1011945222010

Ivanov, B. A., Neukum, G., Bottke, W. F., & Hartmann, W. K. (2002). The comparison of size-frequency distributions of impact craters and asteroids and the planetary cratering rate. Asteroids III.

Malin, M. C., Bell, J. F., Cantor, B. A., Caplinger, M. A., Calvin, W. M., Clancy, R. T., Edgett, K. S., Edwards, L.,

Haberle, R. M., James, P. B., Lee, S. W., Ravine, M. A., Thomas, P. C. & Wolff, M. J. (2007). Context camera investigation on board the mars reconnaissance orbiter. *Journal of Geophysical Research E: Planets*, *112*(5), https://doi.org/10.1029/2006JE002808

Mandon, L., Parkes Bowen, A., Quantin-Nataf, C., Bridges, J. C., Carter, J., Pan, L., Beck, P., Dehouck, E., Volat, M., Thomas, N., Cremonese, G., Tornabene, L. L., & Thollot, P. (2021). Morphological and spectral diversity of the clay-bearing unit at the ExoMars landing site Oxia Planum. *Astrobiology*, *21*(4), 464–480. https://doi.org/10.1089/ast.2020.2292

Neukum, G., Ivanov, B. A., & Hartmann, W. K. (2001). Cratering records in the inner solar system in relation to the lunar reference system. *Space Science Reviews*, *96*(1/4), 55–86. https://doi.org/10.1023/A:1011989004263

Newsom, H. E., Mangold, N., Kah, L. C., Williams, J. M., Arvidson, R. E., Stein, N., Ollila, A. M., Bridges, J. C., Schwenzer, S. P., King, P. L., Grant, J. A., Pinet, P., Bridges, N. T., Calef, F., Wiens, R. C., Spray, J. G., Vaniman, D. T., Elston, W. E., Berger, J. A., … Palucis, M. C. (2015). Gale crater and impact processes – curiosity's first 364 sols on mars. *Icarus*, *249*. https://doi.org/10.1016/j.icarus.2014.10.013

Osinski, G. R., Tornabene, L. L., Banerjee, N. R., Cockell, C. S., Flemming, R., Izawa, M. R. M., McCutcheon, J., Parnell, J., Preston, L. J., Pickersgill, A. E., Pontefract, A., Sapers, H. M., & Southam, G. (2013). Impact-generated hydrothermal systems on earth and mars. *Icarus*, *224*(2), 347–363. https://doi.org/10.1016/j.icarus.2012.08.030

Quantin-Nataf, C., Carter, J., Mandon, L., Thollot, P., Balme, M., Volat, M., Pan, Lu, Loizeau, Damien, Millot, Cédric, Breton, Sylvain, Dehouck, Erwin, Fawdon, Peter, Gupta, Sanjeev, Davis, Joel, Grindrod, Peter M., Pacifici, Andrea, Bultel, Benjamin, Allemand, Pascal, Ody, Anouck, … Broyer, J. (2021). Oxia Planum: The landing site for the ExoMars "Rosalind Franklin" rover mission: Geological context and prelanding interpretation. *Astrobiology*, *21*(3), 345–366. https://doi.org/10.1089/ast.2019.2191

Quantin-Nataf, C., Craddock, R. A., Dubuffet, F., Lozac'h, L., & Martinot, M. (2019). Decline of crater obliteration rates during early Martian history. *Icarus*, *317*, 427–433. https://doi.org/10.1016/j.icarus.2018.08.005

Robbins, S. J., & Hynek, B. M. (2012). A new global database of mars impact craters ≥1 km: 2. Global crater properties and regional variations of the simple-to-complex transition diameter. *Journal of Geophysical Research E: Planets*, *117*(6), https://doi.org/10.1029/2011JE003967

Schwenzer, S. P., Abramov, O., Allen, C. C., Clifford, S. M., Cockell, C. S., Filiberto, J., Kring, D. A., Lasue, J., McGovern, P. J., Newsom, H. E., Treiman, A. H., Vaniman, D. T. & Wiens, R. C. (2012). Puncturing mars: How impact craters interact with the Martian cryosphere. *Earth and Planetary Science Letters*, 335–336. https://doi.org/10.1016/j.epsl.2012.04.031

Smith, D. E., Zuber, M. T., Frey, H. V., Garvin, J. B., Head, J. W., Muhleman, D. O., Pettengill, G. H., Philips, R. J., Solomon, S. C., Zwally, J., Banerdt, W. B., Duxbury, T. C., Golombek, M. P., Lemoine, F. G., Neumann, G. A., Rowlands, D. D., Aharanson, O., Ford, P. G., Ivanov, A. B..., Sun, X. (2001). Mars Orbiter Laser Altimeter: Experiment summary after the first year of global mapping of mars. *Journal of Geophysical Research E: Planets*, *106*(E10), https://doi.org/10.1029/2000JE001364

Southam, G., Westall, F., & Spohn, T. (2015). Geology, life, and habitability. *Treatise on Geophysics: Second Edition*, *10*. https://doi.org/10.1016/B978-0-444-53802-4.00175-5

Strom, R. G., Croft, S. K., & Barlow, N. G. (2018). The Martian impact cratering record. *Mars*, https://doi.org/10.2307/j.ctt207g59v.16

Sweeney, J., Warner, N. H., Golombek, M. P., Kirk, R., Fergason, R. L., & Pivarunas, A. (2016, March 21-25). *Crater degradation and surface erosion rates at the insight landing site, western elysium planitia, mars*. 47th Lunar and Planetary Science Conference, held in the Woodlands, Texas.

Tanaka, K. L., Skinner, J. A., Dohm, J. M., Irwin, R. P., Kolb, E. J., Fortezzo, C. M., Platz, T., Michael, G. G. & Hare, T. M. (2014a). Geologic Map of Mars. U.S. Geological Survey Geologic Investigations.

Tanaka, K. L., Skinner, J. a., Dohm, J. M., Irwin, R. P., Kolb, E. J., Fortezzo, C. M., Platz, T., Michael, G. G. & Hare, T. M. (2014b). Geologic Map of Mars (Scientific Investigations Map 3292). U.S. Geological Survey Geologic Investigations.

Vago, J. L., Westall, F., Coates, A. J., Jaumann, R., Korablev, O., Ciarletti, V., Mitrofanov, I., Josset, J., De Sanctis, M. C., Bibring, J., Rull, F., Goesmann, F., Steininger, H., Goetz, W., Brinckerhoff, W., Szopa, C., Raulin, F., Westall, F, Edwards, H. G. M..., the ExoMars Project Team. (2017). Habitability on early mars and the search for biosignatures with the ExoMars rover. *Astrobiology*, https://doi.org/10.1089/ast.2016.1533